Vibrotactile Sensitivity Threshold: Nonlinear Stochastic Mechanotransduction Model of Pacinian Corpuscle

Abhijit Biswas, M. Manivannan and M. A. Srinivasan

Abstract—Based on recent discoveries of stretch and voltage activated ion-channels present in the receptive area of Pacinian-corpuscle (PC), this paper describes a novel two-stage nonlinear mechanotransduction model of vibrotactile-sensitivity-threshold (VTST), valid over a wide frequency-band of 10 Hz to few kHz. The model is based on the nonlinear and stochastic behaviour of ion-channels represented as dependent-charge-sources loaded with membrane impedance. It accurately simulates the neural-response of PC around threshold considering the morphological and statistical properties of receptor-potential and action-potential with the help of adaptive-relaxation-pulse-frequency-modulator (ARPFM). This model also simulates the plateaus and nonmonotonic saturation of spike-rate characteristics. The stochastic simulation based on additional mechanical and neural noise clearly describes that VTST at higher frequency is more dependent on noise than at lower frequency range. Therefore even SNR=150 improves neurophysiological-threshold by more than 3 dBμ above 400 Hz. However above 800 Hz the absence of entrainment-thresholds and relatively lower sensitivity-index near absolute-threshold makes the upper-bound of the psychological-VTST more dependent on experimental-protocol and physical-setup. This model can be extended to simulate neural-response of a group of PCs, for finding the optimum transformation of the speech-signal to interface speech through skin for the hearing impaired, as it partly covers the speech-frequency band.

Index Terms—Neurophysiology, Ion channel dynamics, Receptor potential, Adaptive relaxation pulse frequency modulation

1 Introduction

Human Vibro-Tactile (VT) sensitivity is rarely studied analytically covering few 10s of Hz to few kHz using a single model. One of the requirements of such a study stems from the development of better techniques for conveying speech and visual information through somatosensory channel [1], [2]. Although VT displays typically uses frequency band below 400 Hz, they may function till 2000 Hz as Vibrotactile Sensitivity Threshold (VTST) till 2000 Hz is found to be around 0.5 to 100 μm [3], [4], [5], [6], [7], [8], [9], [10], [11]. These VTST characteristics (VTSTCs) can be classified into either neurophysiological (considering the response of individual mechanoreceptors [8], [12]) or psychophysical (considering the overall stimulus detectability of skin [3], [7]) characteristics. Though there are numerous VTSTCs, there are very few attempts to theoretically analyze the variations in the two classes of VTSTCs with the help of a single model covering the full bandwidth of VTSTC.

In order to describe the complete mechanosensory system, [13], [14] proposed an equivalent model of PC by cascading three blocks: a differentiation block (to represent the mechanical signal processing in PC layers), rectification with band pass filtration (BPF) block (to represent the electro-mechanical transduction in PC inner core) and neural spike conversion block (to represent the neural activity in PC core membrane and in the axon). Though the neural spike generator can be electrochemically modeled in great details [12], [15], recent literature [13], [16], [17], [18] hint that the binary spike generation of the sensory receptors can be quite accurately modeled with Integral Pulse Frequency Modulator (IPFM) or Relaxation Pulse Frequency Modulator (RPFM). However the existing RPFM models [16], [17], [18] capture only the binary spikes in order to match the experimental spike rate. Moreover they can not accurately capture PC neural response over a wide spectrum [17]. In this paper we present a nonlinear two stage mechanotransduction model along with Adaptive RPFM (ARPFM) that not-only simulates the binary spike rate, but also morphological and statistical parameters of the neurophysiological signals of intermediate stages involved in vibrotactile sensation, starting from the mechanical stimulus to the perception of vibration.

The novelties of the proposed model described in this paper are as follows: (1) Two stage nonlinear mechanotransduction considering the stretch and voltage activated ion channels present in the receptive area of PC neurite [19]; (2) Analytical estimation of the ARPFM threshold amplification characteristic and its effect on the morphology and statistics of neural spike train; (3) Evaluation of the effect of neural noise on generated spike train over a wide spectrum; (4) Characterization of the grouping of neural spikes; (5) Estimation of VTST from neural spike rate of binary spike train; and (6) Description of noise dependency of VTST especially above 400 Hz.

• *A. Biswas and M. Manivannan are with the TouchLab, Biomedical Research Group, Department of Applied Mechanics, IIT Madras, Chennai, India. Email: mani@iitm.ac.in*
• *M. A. Srinivasan is with the TouchLab, The Research Laboratory of Electronics, Massachusetts Institute of Technology, Cambridge, MA 02139, USA. Email: srini@mit.edu*

Manuscript submitted 16 Aug. 2013; revised 21 Mar. 2014

2 Model Description and Method

The proposed model considers PC as the only mechanoreceptor, as the main objective of this paper is to develop a unified framework of biomechanical, neurophysiological and psychophysical signal processing associated with the human VT sensitivity over a wide frequency range above 10s of Hz. Fig. 1 shows the schematic of biomechanical and neuphysiological signal processing which converts the mechanical signal applied on skin to the neural spike train.

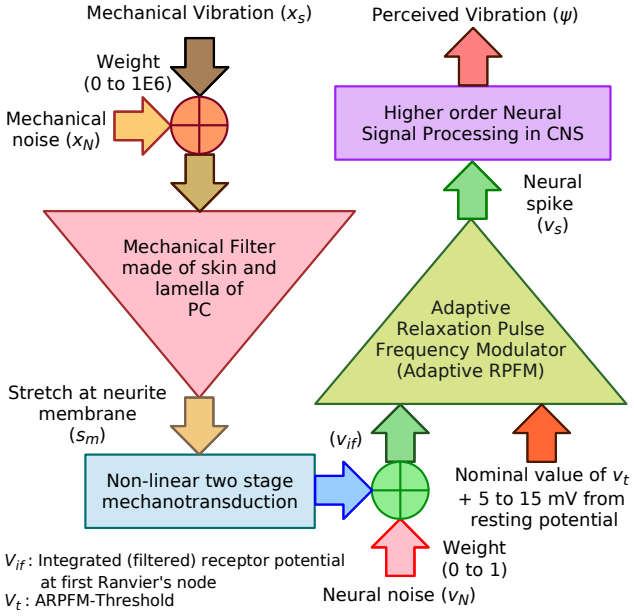

Fig. 1. Schematic of overall simulation of neural response of PC starting from the mechanical excitation.

2.1 Layered biomechanical model of skin & PC

The biomechanical model used in this paper consists of PC and skin layers, detailed in [20], [21] along with the approximations. For the sake of completeness the model is briefly described in this section. The PC in the skin column is embedded between dermis and hypodermis. As [22] shows VTST do not vary significantly when the indenter diameter is above 1 mm, the diameter of the skin column in the model is also chosen as 1 mm, which is slightly larger than the dimension of a PC.

The compression of the PC inner core ($w_c(t)$) primarily controls the neural activity of PC, therefore to obtain $w_c(t)$ we have used two dimensionless transfer functions named as Compression Transmittance Transfer Function (CTTF) $N_{sp}(s)$ and $N_{pn}(s)$. $N_{sp}(s)$ relates the compression of the PC outer layer ($w_p(t)$) to the displacement of the skin outer layer ($x_s(t)$) and $N_{pn}(s)$ relates the deformation of the PC core (0^{th}) layer ($w_c(t)$) to the compression of the PC outer most (n^{th}) layer ($w_p(t)$) (referred in supplementary material). In this paper $w_c(t)$ is fed to the mechanotransduction block through a constant gain λ=0.01 representing the stretch signal at the membrane of neurite $s_m(t)$ in Fig 2. The chosen value of λ is a reasonable approximation, which can be ratiometrically scaled with mechanotransduction characteristics (1) described in next section.

2.2 Mechanotransduction and Adaptive RPFM

Mechanotransduction and neural spike generation at the 1st Ranvier's node of PC are modeled by two stage nonlinear signal processing (Fig. 2), where the 3rd stage is the Adaptive Relaxation Pulse Frequency Modulation (ARPFM) [16], [18].

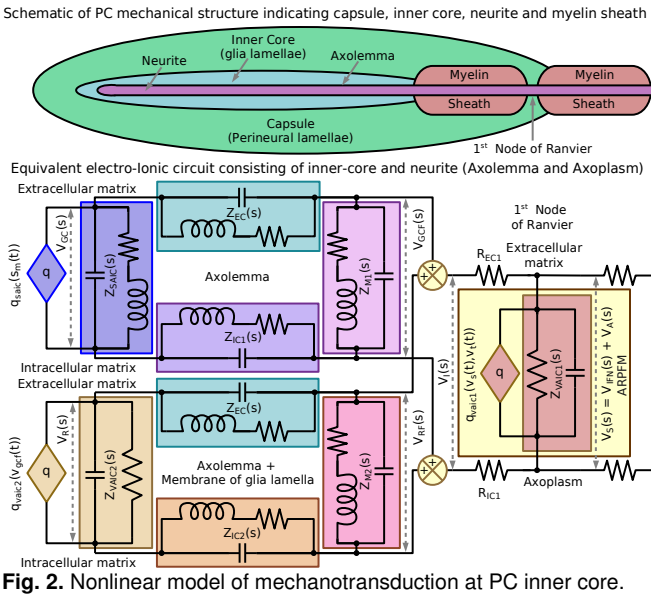

Fig. 2. Nonlinear model of mechanotransduction at PC inner core.

The plethora of Stretch Activated Ion Channels (SAIC) [23] present in PC can be broadly classified into low threshold (LT) and high threshold (HT) channels [24]. The LT channels (pressure threshold ~ 2 kPa) are found to be sensitive to both +ve and -ve pressure gradient w.r.t. the extracellular matrix and the sensitivity increases till ±13 kPa [24]. On the other hand the HT channels have threshold at -8 kPa and found to be insensitive till +13 kPa. It even appears that the LT channels are little more abundant than the HT channels [24].

Two stages of nonlinear receptor potential generation: In order to use the experimental results of [24] in this model, the +ve pressure is mapped to -ve stretch of neurite membrane ($s_m^n(t)$) and -ve pressure is mapped to the +ve stretch ($s_m^p(t)$). The stretch excitation to neurite membrane ($s_m(t)$) results the 1st stage of generator potential which incorporates two levels of nonlinearities as detailed in the following section. However, 2nd stage contains only one level of nonlinearity in generation of the receptor potential from the secondary voltage excitation as described later. While the 1st stage models the SAICIs the 2nd stage models the nonlinear amplification of the 1st stage generator potential by the Voltage Activated Ion Channels (VAICs). Although the term generator potential is used synonymously to the receptor potential in this paper, it mostly represents the 1st stage of receptor potential.

1st stage 1st level: The transduction characteristics of the stretch on membrane ($s_m(t)$) to the overall charge transfer through the SAIC ($q_g(t)$) is considered as the nonlinear dependent charge source (or current source), described by the function ($q_g(t)=q_{saic}(s_m(t))$), as shown in Fig. 3A. The function $q_{saic}(s_m(t))$ is chosen based on the probability of an ion channel (HT and LT) opening under certain $s_m(t)$ [24], [25] and shown Fig. 3A and (1). The term $q_g(t)$ indicates the net influx of the +ve ions through SAICs due to direct stretch excitation. On macro scale $q_g(t)$ vs. $s_m(t)$ resembles a nonlinear full wave rectification characteristics, but it may appear as half-wave rectification or exponential saturation characteristics depending on the operating point and range. In the nonlinear expression of the each component of $q_g(t)$ (1) the α controls the threshold, β controls near-threshold sensitivity and τ controls the creep for the supra-threshold stimulus. The value of k is chosen as 4 based on the number of decades of supra-threshold stimulus amplitude to be simulated. The saturation level of $q_g(t)$ is controlled by the coefficient (φ).

$$q_g(t) = q^p_{gL}(t) + q^n_{gL}(t) + q^p_{gH}(t) + q^n_{gH}(t); \quad \textit{where}$$

$$q^p_{gL}(t) = \varphi^p_L \left(1-\exp\left(-\left(\frac{s^p_m(t)}{\alpha^p_L}\right)^{\beta^p_L}\right)\right)\frac{1}{k}\sum_{i=0}^{k}\left(1-\exp\left(\frac{-s^p_m(t)}{10^i\tau^p_L}\right)\right) \quad (1)$$

$q^n_{gL}(t)$ and $q^p_{gH}(t)$ are similar to $q^p_{gL}(t)$ and $q^n_{gH}(t)=0$

$\varphi^p_L = 5.0\text{e-}11\,C$, $\alpha^p_L = r_0 6\text{e-}5\,\mu m$, $\beta^p_L = 5$ and $\tau^p_L = \alpha^p_L 1\text{e}2$

$\varphi^n_L = 5.0\text{e-}11\,C$, $\alpha^n_L = r_0 2\text{e-}4\,\mu m$, $\beta^n_L = 9$ and $\tau^n_L = \alpha^n_L 8\text{e}1$

$\varphi^p_H = 2.5\text{e-}11\,C$, $\alpha^p_H = r_0 2\text{e-}3\,\mu m$, $\beta^p_H = 4$ and $\tau^p_H = \alpha^p_H 1\text{e}4$

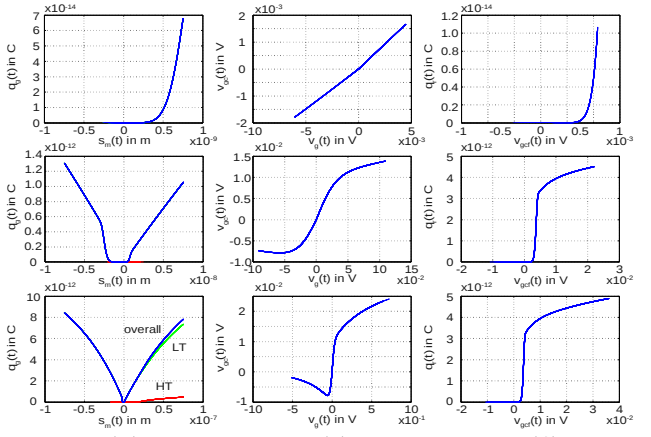

Fig. 3. Nonlinear transduction characteristics for different range of stimulus amplitude (in column: just sub-threshold, supra-threshold, complete-saturation); **(A)** Characteristics relating stretch in neurite membrane ($s_m(t)$) to charge transfer through axolemma $q_g(t)$ due primary excitation to stretch activated ion channels (SAICs); **(B)** Characteristics describing clipping of 1st stage generator potential $v_g(t)$; **(C)** Characteristics relating clipped & filtered 1st stage generator potential ($v_{gcf}(t)$) to the secondary transmembrane charge transfer $q_t(t)$ due to excitation to the voltage activated ion channels (VAICs).

Apart from non-linearity between $q_g(t)$ vs. $s_m(t)$, the LT and HT ion channels have different temporal responses; while LT is slower, HT is faster [24]. A certain population of LT ion channels has average closing time constant remains in the order of 1.5 ms and can creep up to 10 ms [24]. On the other hand, the opening time constant of LT channels is 4-times lower than that of closing. Compared to LT channels, HT channels have more identical opening and closing time constants [24]. In general the time constant for enabling the SAICs are reported to be in the order of 0.5 and 2.5 ms [25]. Therefore the internal impedance (Fig. 2) of the overall SAICs ($Z_{SAIC}(s)$) are modeled as 2nd order transfer function with a little under-damped pole-pair and a zero as given in (2). The $q_g(t)$ generates the first stage of generator potential $v_g(t)$, based on the complex-elastance ($E_{SAIC}(s) = s * Z_{SAIC}(s)$) of the SAIC.

$$Z_{SAIC}(s) = \frac{V_G(s)}{sQ_G(s)} = \frac{5.0\text{e}7\,(2\pi 400)^2\left(1+\frac{s}{2\pi 390}\right)}{s^2 + 2(0.30)(2\pi 400)s + (2\pi 400)^2} \quad (2)$$

1st stage 2nd level: As the SAICs are themselves voltage sensitive and they conducts under both +ve and -ve voltage excitation, $v_g(t)$ experiences 2nd level of nonlinearity in the form of clipping. Under +ve voltage excitation SAICs mostly saturates exponentially, but under -ve voltage excitation their conduction shows different type of clipping with a higher order non-linearity [23], [24], [26], [27], [28], [29]. The clipping characteristic for PC neurite is chosen based on [26] and its analytical form is given in (3) (Fig. 3B). The clipped version of the $v_g(t)$ ($v_{gc}(t)$) represents the effective EMF (open-load voltage) of the SAICs in the receptive area of PC neurite.

$$v_{gc}(t) = v^{max}_{gc}\left(v^t_{gc}(t) + v^e_{gc}(t)\right)/(2k)$$

$$v^t_{gc}(t) = tansig\left(\frac{v_g(t)}{\tau_g}\right) + \sum_{i=2}^{k} tansig\left(\frac{v_g(t)}{10^i\tau_g}\right);$$

$$v^e_{gc}(t) = \sum_{i=1}^{k-1}\left(1-\exp\left(\frac{-v^p_g(t)}{10^i\tau_g}\right)\right) + \sum_{i=1}^{k}\left(1-\exp\left(\frac{v^n_g(t)}{10^i\tau_g}\right)\right); \quad (3)$$

where $v^p_g(t)$ and $v^n_g(t)$ are +ve and -ve part of $v_g(t)$,

$v^{max}_{gc} = 0.1\,V$, $\tau_g = 0.3\,V$ and $k = 5$

Loading effect of neurite membrane: Similar to $Z_{SAIC}(s)$ the longitudinal and transverse membrane impedance is also frequency dependent which can be modeled as frequency dependent capacitor [30] or as RLC combination [31] (Fig. 2). Considering the electrical loading effect of extracellular fluid, neurite membrane and intracellular fluid the observable form of the 1st stage generator potential ($v_{gcf}(t)$) is derived from the effective EMF of the SAICs ($v_{gc}(t)$). Therefore the initiated potential $v_{gc}(t)$ is filtered by the assembly of $Z_{EC}(s) \leftrightarrow Z_{M1}(s) \leftrightarrow Z_{IC1}(s)$ as shown in Fig. 2, which acts as a bi-proper 2nd order filter ($TR_1(s)$) expressed in (4). The constituents $TR_1(s)$ are considered as 2nd order transfer functions similar to $Z_{SAIC}(s)$ based on [31]. Such transfer functions quite accurately model the longitudinal impedance of neural membrane. Due to the presence of significant amount of SAIC in the receptive area of axolemma, $Z_{M1}(s)$ is also modeled as 2nd order.

$$TR_1(s) = \frac{V_{GCF}(s)}{V_{GC}(s)} = \frac{0.9(2\pi 150)^2\left(1+\frac{s}{2\pi 50}\right)\left(1+\frac{s}{2\pi 1\text{e}4}\right)}{s^2 + 2(0.70)(2\pi 150)s + (2\pi 150)^2} \quad (4)$$

2nd stage of Mechanotransduction: The 1st stage of generator potential $v_{gcf}(t)$ while spreading through the membranes inside the inner core gives raise to 2nd stage of receptor potential $v_r(t)$ by the VAICs. Due to $v_{gcf}(t)$ the net inflow of +ve charge $q_r(t)=q_{VAIC2}(v_{gcf}(t))$ (5) gives rise to $v_r(t)$ depending on $Z_{VAIC2}(s)$ (6) and becomes significant whenever $v_{gcf}(t)$ reaches close to the nominal threshold of VAICs (Fig. 3C). The characteristics of the nonlinear voltage dependent charge source (or current source) $q_r(t)=q_{VAIC2}(v_{gcf}(t))$ is depicted in Fig. 3C.

$$q_r(t)=q_r^m\left(1-\exp\left(-\left(\frac{v_{gcf}^p(t)}{\alpha_r}\right)^{\beta_r}\right)\right)\frac{1}{k}\sum_{i=0}^{k}\left(1-\exp\left(\frac{-v_{gcf}^p(t)}{10^i\tau_r}\right)\right) \quad (5)$$

$q_r^m = 9.0\text{e-}12\,C$, $\alpha_r = v_{thd}^{nom}75\,\%$, $\beta_L^p = 10$ and $\tau_L^p = \alpha_r 0.1$

$$Z_{VAIC2}(s)=\frac{V_R(s)}{s\,Q_R(s)}=\frac{4.0\text{e}11}{\left(1+\frac{s}{2\pi 0.01}\right)} \quad (6)$$

Loading effect of axolemma and lamellae membrane: In contrary to the $v_g(t)$, not only the axolemma takes part in generation of $v_r(t)$ but also the membrane of glia lamellae and probably the perineural lamellae, as they too have VAICs [19]. Therefore the transfer function for $Z_{M2}(s)$ and $Z_{IC2}(s)$ is different than that of the 1st stage as they represent the combined effect of neurite and the lamellae. Similar to the 1st stage, the assembly of $Z_{EC}(s) \leftrightarrow Z_{M2}(s) \leftrightarrow Z_{IC2}(s)$ construct another bi-proper 2nd order filter ($TR_2(s)$) for $v_r(t)$ (Fig. 2) and its expression is given in (7). The observable form of the overall receptor potential is effectively the summation of the filtered $v_{gc}(t)$ and $v_r(t)$, which is denoted as $v_i(t) = v_{gcf}(t) + v_{rf}(t)$.

$$TR_2(s)=\frac{V_{RF}(s)}{V_R(s)}=\frac{0.4(2\pi 350)^2\left(1+\frac{s}{2\pi 200}\right)\left(1+\frac{s}{2\pi 1\text{e}4}\right)}{s^2+2(0.80)(2\pi 350)s+(2\pi 350)^2} \quad (7)$$

As shown in Fig. 2, all the 2nd order impedances considered in the model reduces to 1st order if the inductance is neglected. In the discussion section we have described the importance and the possible origin of such under-damped 2nd order impedance associated with mechano-sensitive cell membrane.

Adaptive RPFM (ARPFM): The spike generation at 1st Ranvier's node of PC can be modeled with ARPFM (Fig. 1 and 2), which is functionally different from the model of VAICs of the receptive area as described in the following section. The main difference is the adaptive threshold characteristics of ARPFM resulted by the refractoriness and rapid adaptiveness of the Na^+ VAICs of 1st Ranvier's node. The ARPFM is similar to integrate-and-fire model [16], [17] but different in two aspects: 1) the integrator is lossy (realized with a Low Pass Filter (LPF)), and 2) the relaxation frequency modulator includes an adaptive threshold ($v_t(t)$) which is physiologically more intuitive representation of refractoriness than the *integrator discharge current*. The ARPFM as described in this paper captures the shape of action potential more accurately than integrate-and-fire model.

LPF of ARPFM: The presence of lossy integrator (or 1st order LPF) in ARPFM offers the temporal summation for the signal above cutoff frequency. In contrary to ideal integrator (cutoff = 0 Hz), output of lossy integrator does not ramp over a long time for the signals below cutoff frequency. In our model the LPF cutoff is set in the range of 15 to 20 Hz in contrary to 0.8 Hz of [32], which is found to be more reasonable in comparison to the membrane impedance (Fig. 2). It also offers better matching of the shape of receptor potential ($v_{if}(t)$) at 1st Ranvier's node of PC. In our model lowering the cutoff further not only alters the shape of $v_{if}(t)$ but also affects the accuracy of the generated spike train for trapezoidal and sinusoidal stimulus as width of 1st tuning plateau reduces. On the other hand increasing this cutoff above 200 Hz also reduces the width of the 1st tuning plateau making the $v_{if}(t)$ taller (close to 100 mV) and narrower while attempting to match the desired level of saturation spike rate for stimulus ~100 Hz. According to the schematic (Fig. 2), $R_{EC1}(s) \leftrightarrow Z_{VAIC1}(s) \leftrightarrow R_{IC1}(s)$ forms the LPF and the transfer function of the filter ($TR_3(s)$) is given in (8). The final constraint in tuning this cutoff of the ARPFM LPF comes from the peak value of the $v_{if}(t)$ that is observed in experiment [26], [33], [34]. Typically $v_{if}(t)$ saturates around +50 mV from resting membrane potential. On the other hand cell membrane has typically dielectric breakdown voltage ~200 mV [35] and therefore none of the neurophysiological voltage signals practically reaches close to it. This criterion is well satisfied at all the stages of electro-ionic signal processing. It is worth noting that all the membrane potential mentioned in the following section are referenced to the resting membrane potential (-70 mV approx.).

$$TR_3(s)=\frac{V_{if}(s)}{V_i(s)}=\frac{1}{\left(1+\frac{s}{2\pi 17.8}\right)} \quad (8)$$

Threshold of ARPFM: The ARPFM threshold is actually a measure of the refractoriness of the Na^+ VAICs to go for the next avalanche opening. In comparison to the model of VAIC, as ARPFM the threshold ($v_t(t)$) is adaptive and amplified by the threshold amplification factor in the refractory period as found in [34] and shown in Fig. 4. The analytical form of adaptive threshold ($v_t(t)$) as estimated from [34] represents the amplification factor w.r.t. its nominal value v_{t_nom} = ~5 mV in the time frame starting from the instantaneous crossing of $v_{if}(t)$ over $v_t(t)$ (t=0 for current time frame). In order to extrapolate $v_t(t)$ towards the absolute refractory period, two different forms of equations are chosen and their possible variations (1-3 and 4-8) are depicted in Fig. 4. These two forms inherently satisfy two basic properties of the ARPFM threshold amplification characteristics: 1) they tend towards infinity for a small duration after initiation of a neural spike *(t=0 for current time frame)*, and 2) fall exponentially towards unity as $t \to \infty$ for any value of the coefficients. It is ob-

served that after 2.5 ms the experimental data have an exponential decay with time constant of 0.56^{-1} ms (pole at 89 Hz w.r.t. Laplace transform) and therefore in the 2nd form of equation contains same exponential factor (Fig. 4).

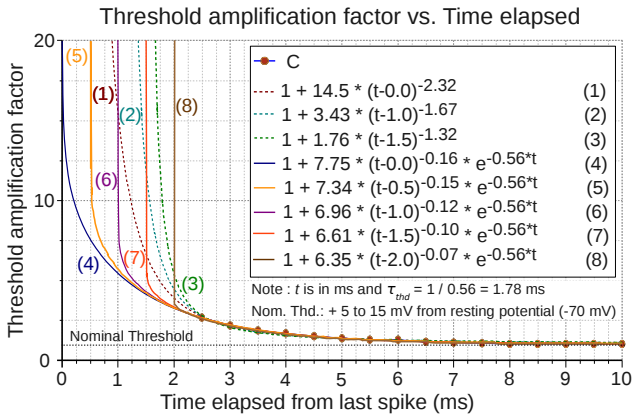

Fig. 4. Threshold amplification characteristics of ARPFM.

Choice of ARPFM threshold: The key factor in choosing a particular analytical expression of ARPFM threshold as shown in Fig. 4 is the fact that once an Na^+ VAIC completely opens, it can not be reopened unless the membrane hyper-polarizes and there is very little probability that an Na^+ channel remained closed during the previous action potential. As the typical time constant for hyper-polarization from the initiation of depolarization of the membrane is about 1.5 ms, the characteristic 7 of Fig. 4 is found to be most suitable for ARPFM. Due to the rapid recovery after 1.5 ms, characteristic 7 can also offer the saturation spike rate just around 550 sps (spikes per second), which matches most of the experimental results [8], [36]. At the same time it completely eliminates the probability of triggering next action potential in repolarization phase as $v_t(t) \rightarrow \infty$ for the duration of 1.5 ms from the triggering instant of last action potential (t=0). Characteristics 1, 2 and 8 offers relatively higher value of $v_t(t)$ in the time duration of 1.5 to 2.5 ms limiting the saturation spike rate of the PC below 500 sps. The characteristics 4, 5 and 6 allows generation of next action potential in the repolarization phase, which are supposed to be merged with the last action potential itself. However characteristics 6 can be next best choice which can offer saturation spike rate of 800 sps but occasionally it triggers spikes in repolarization phase, which causes an error in calculation of binary spike rate and significantly distorts the shape of action potential in those cases.

Shape of action potential: The generation of action potential can be very accurately modeled using ARPFM, including the shape. The instantaneous crossover of $v_{if}(t)$ w.r.t. $v_t(t)$ actually triggers the avalanche opening of the Na^+ VAICs. The trigger ($v_{at}(t)$) is considered as an unit impulse function, approximated by rectangular pulse of 0.2 ms which is the typical time constant for opening a Na^+ VAIC [37]. Depending upon the transfer function $TF_{Na}(s)$ as given in (9), $v_{at}(t)$ results in the ionic potential $v_{Na}(t)$ which is in-fact the impulse response of Na^+ VAICs. Similarly, same trigger $v_{at}(t)$ generates the impulse response of K^+ VAICs based on $TF_K(s)$ given in (10). It is worth noting that $TF_K(s)$ contains a delay of 0.4 ms in it. The net action potential ($v_a(t)$) is considered as $v_a(t)=v_{Na}(t)-v_K(t)$. The natural frequencies of $TF_{Na}(s)$ and $TF_K(s)$ acts similar to the carrier frequency of a frequency modulator. The net observable potential (neural spike train) ($v_s(t)$) at 1st Ranvier's node is the superposition of the $v_a(t)$ and $v_{if}(t)$. The binary form of $v_s(t)$ is referred as $v_{spk}(t)$ in later sections.

$$TF_{Na}(s) = \frac{V_{Na}(s)}{V_{AT}(s)} = \frac{A_{Na}\,\omega_{Na}^2}{s^2 + 2\delta_{Na}\omega_{Na}s + \omega_{Na}^2};\ \text{where} \quad (9)$$

$$A_{Na} = 1.33\text{e-}4,\ \delta_{Na} = 0.85 \text{ and } \omega_{Na} = 2\pi 350\, rad/s$$

$$TF_K(s) = \frac{V_K(s)}{V_{AT}(s)} = \frac{A_K\,\omega_K^2\, e^{-0.0004s}}{s^2 + 2\delta_K\omega_K s + \omega_K^2};\ \text{where} \quad (10)$$

$$A_K = 1.33\text{e-}4,\ \delta_K = 0.70 \text{ and } \omega_K = 2\pi 200\, rad/s$$

The advantage of modeling the neural spike generation with ARPFM is that the $v_t(t)$ takes care of the group of VAICs, and $TF_{Na}(s)$ and $TF_K(s)$ takes care of how the shape of action potential should be after recovery period as well as within refractory period. Therefore it offers desired accuracy w.r.t. the shape and height variation of the action potential in the relative refractory period.

2.3 Model of noise

As shown in Fig. 1, this model includes mechanical and neural noise separately. The reason behind these two separate provisions is that the nonlinear signal processing in mechanotransduction and ARPFM alters the statistical and morphological properties of mechanical noise ($x_N(t)$) and neural noise ($v_N(t)$) differently.

Mechanical noise: For simplicity the mechanical noise ($x_N(t)$) is considered as pseudo-Gaussian noise with SD = 0.1 µm and filtered with 1 kHz cutoff 1st order LPF. This results in the RMS of $x_N(t)$ equal to 5.5e-3 µm and also offers SNR > 1.5 even for the weakest signal (0.01 µm amplitude sine wave) considered for simulation. The weight on the noise (Fig. 1) is varied from 0 dB to 30 dB in steps of 5 dB and a special case (noise weight=0). However for simulating the response of PC against noise alone, the RMS of $x_N(t)$ is varied from 0.01 to 1000 µm while keeping the noise-weight = 1.

Neural noise: For the ARPFM the neural noise is modeled as an additive random noise $v_N(t)$ which can be associated either with the adaptive threshold ($v_t(t)$) or with the filtered receptor potential ($v_{if}(t)$). We have assumed that noise $v_N(t)$ does not scale up with the signal or with the threshold, providing better SNR for stronger signal. In reality, however it may not be strictly satisfied due to nonlinear and stochastic nature of mechanotransduction. The random neural noise $v_N(t)$ typically consists of two types of random noises [18]: Pulsating noise $v_{NP}(t)$ and Gaussian noise $v_{NG}(t)$. $v_{NP}(t)$ represents the random leakage of ions through the cell membrane, modeled as

pulsating biphasic signal with the height of nominal threshold and duration of 0.1 ms, with an average occurrence rate of 1 in 1 ms. This noise signal is filtered using a 1st order LPF having a time constant of 1.78 ms which is same as the exponential decay constant of threshold amplification factor (τ_{thd}) as shown in Fig. 4. On the other hand $v_{NG}(t)$ represents the Johnson thermal noise and modeled as additive Gaussian noise with SD same as the nominal ARPFM threshold voltage level (Fig. 4) and filtered using 1st order LPF having time constant one fifth of τ_{thd} (cutoff frequency = 450 Hz).

In order to illustrate some idealistic responses of the model, we have considered a special configuration of zero weight for mechanical and neural noise and referred it as deterministic model in the following sections. The term stochastic model represents the configuration where the mechanical and neural noise-weight is considered nonzero (Fig. 2).

2.4 Estimation of VT sensory threshold

The basic approach in estimating the VTST from deterministic model is to find the minimum amplitude of stimulus applied on skin outer layer ($x_S(t)$) which results in nonzero spike rate. The spike rate is determined based on a 300 ms window. There are three reasons behind choosing 300 ms frame: 1) above 300 ms duration, temporal framing of stimulus does not alter its detectability [38], 2) the histogram analysis of the spike trains shows that rarely two spikes make a larger time gap than 250 ms in presence of noise, which is also observed in [8], and 3) 300 ms frame fits significant number of stimulus cycles for the frequency range of 12.5 to 3200 Hz.

In order to find the threshold amplitude of $x_S(t)$ an iterative computation is followed for the frequency range of 12.5 to 3200 Hz, doubling in each step. The amplitude of $x_S(t)$ is varied from 0.01 to 1000 µm for each of the selected frequencies. The estimation of VTSTC from the deterministic model is based on zero-crossing of spike rate and denoted as *SR_DT=0sps* in the following sections (SR: *Spike Rate*, _DT: *Deterministic*, sps: *spike per second*).

In case of stochastic model, as spike rate never touches zero, the zero-crossing approach of estimating VTST fails. Therefore conceptually threshold amplitude of $x_S(t)$ should indicate the cross-over of the deterministic component of spike train ($v_{spk}(t)$) over its stochastic component. One of the techniques to identify the deterministic component of the neural spike train near the threshold is proposed by Freeman and Johnson [12] considering the probability of generating two neural spikes in consecutive two stimulus cycles. However this technique fails above 400 Hz, as this probability remains close to zero even for the significantly supra-threshold stimulus; this is due to the saturation that keeps the spike rate several times lower than the stimulus frequency [8], [36]. In this high frequency band, the deterministic component of the neural spike train remains largely incoherent to the phase of the stimulus in spite of being supra-threshold. Therefore, instead of observing only two consecutive stimulus cycles, 5 frames of each 300 ms containing more stimulus cycles are observed and Mean, Standard Deviation (SD) and Coefficient of Variation (CV) of spike rate are computed. For convenience, instead of CV, its inverse which is Mean to SD Ratio (MSDR) is considered as a good metric to quantify the deterministic nature of neural spike train ($v_{spk}(t)$). MSDR increases with the stimulus amplitude near threshold while CV decreases. The consistency of the estimated MSDR has been verified by considering ten 300 ms frames. Apart from MSDR, mean spike rate itself indicates the deterministic nature of $v_{spk}(t)$.

In order to quantify psychophysical VTST from binary form of $v_{spk}(t)$, we have fitted a straight line to mean spike rate (SR) vs. stimulus amplitude (SA) data in semi-log scale (11) (Fig. 12); where β is considered as the log of VTST (τ) and α is the VT sensitivity index of PC near the threshold. Above 50 Hz, such straight line can only approximate the SR vs. $\log(SA)$ data within the atonal interval (spike rate lower than stimulus frequency) [39], as the spike rate rapidly gets saturated after the atonal interval in the high frequency range. Therefore for individual frequencies the data points above the spike rate > 200 sps or the stimulus frequency are eliminated for fitting the straight line. Similarly such straight line fitting needs elimination of some data below a threshold which can have a value in-between 0.1 sps to 5 sps [8], [36]. This threshold is set to 0.01 sps, as in this simulation the mechanical noise ($x_N(t)$) can be as low as (5.5e-3 µm rms). For estimating α, only the range of amplitude where all spike rates > 0.01 sps are taken into account. Apart from the absolute VTST (τ), we have also measured the entrainment threshold (the minimum amplitude of $x_S(t)$ that generates spike rate as same as the stimulus frequency) [17].

$$SR = \left[\alpha(\log(SA) - \beta)\right]^{+}; \ \ where \\ \beta = \log(\tau),\ SR = Spike\ Rate,\ SA = Stimulus\ Amplitude \tag{11}$$

3 Results

In order to analyze the variability of VTST over the range of few 10s of Hz to few kHz we have sampled 9 frequencies starting from 12.5 to 3200 Hz doubling in each step. The amplitude range considered for simulation is 0.01 to 1000 µm with a variable sampling (56 discrete amplitudes). Among the 56 samples, amplitudes near the threshold are sampled at high resolution (< 1 dBµ peak) to capture the abrupt rise in the spike rate characteristics. For each of the amplitude and frequency combination, one round of noise-free simulation (300 ms frame) is conducted and the idealistic absolute signal for each stage of mechanotransduction is captured. To analyze how the noise ($v_N(t)$) parameters get altered in different nonlinear transduction stages and how that affects the final spike train, we have simulated $v_N(t)$ five times to capture the true randomness. It appears that due to the nonlinear mechanotransduction the mechanical noise $x_N(t)$ mainly

contributes to the pulsating component ($v_{NP}(t)$) of neural noise by randomizing the height and area of the spikes in $q_r(t)$. While $v_{NP}(t)$ is simulated for every 300 ms frames, mechanical noise is simulated once and used for all 5 frames in order to reduce the simulation duration.

3.1 Signals at Mechanotransduction stages

The results described in the following section is obtained from the simulation of two typical cases 1) PC is embedded at a fixed depth of skin column and stimulus applied on the outer surface of skin column, and 2) the stimulus directly applied on PC outer most layer without skin column. The variation of neural response due the variation of the depth of PC in skin is out of scope of this paper. However it is worth noting that while applying stimulus with skin column, the signals in the range of 300 to 3000 Hz gets attenuated from 0 to 5 dB before reaching PC outer surface (referred in supplementary material).

In order to describe how nonlinearity and stochasticity in mechanotransduction alters the shape of receptor potential ($v_{if}(t)$) and neural spike ($v_s(t)$) at 1st Ranviers's node, a typical sinusoidal and trapezoidal stimuli are shown in Fig. 5 along with the morphological details of intermediate signals. The left column of Fig. 5 A and B represents signals at the receptive area of PC neurite and the right column represents signals at the 1st Ranvier's node.

Left column of Fig. 5 A and B: Both the mechanical stimulus reaching PC core ($w_c(t)$) and the stretch on the neurite membrane ($s_m(t)$) are high-pass filtered form of compression of the PC outermost layer ($w_p(t)$). The charge transferred through the SAICs ($q_g(t)$) resembles a nonlinear rectification of $s_m(t)$. However due to nonlinear relation between $q_g(t)$ and $s_m(t)$, shape of $q_g(t)$ is highly dependent on the amplitude and frequency of the stimulus ($x_s(t)$) and so on $s_m(t)$. Based on the internal impedance of SAICs ($Z_{SAIC}(s)$), only the low frequency components of $q_g(t)$ gets differentiated while generating $v_g(t)$ (Fig. 5). Specifically, below 100 Hz $Z_{SAIC}(s)$ is more resistive and above 400 Hz it becomes more capacitive (2). The observable form of 1st stage generator potential $v_{gcf}(t)$ is shown in Fig. 5 (subplot (5,1) low amplitude trace). The secondary charge transfer $q_r(t)$ by the voltage excitation of the VAICs remains more pulsating than $q_g(t)$ due to the nonlinear characteristics shown in Fig. 3. In contrast to $Z_{SAIC}(s)$, as the $Z_{VAIC}(s)$ remains capacitive even below 1 Hz (6), the shape of the $q_r(t)$ is more or less reproduced in $v_r(t)$. The observable form of 2nd stage receptor potential $v_{rf}(t)$ is shown in Fig. 5 (subplot (7,1) low amplitude trace).

Right column of Fig. 5 A and B: Due to rapid adaptive nature of PC neurite and lamellae membrane, the receptor potential at 1st Ranvier's node ($v_{if}(t)$) contains significant high frequency component (referred as AC) along with the low frequency component (referred as DC). The AC component of ($v_{if}(t)$) rapidly attenuates after 400 Hz making $v_{if}(t)$ flatter which appears to be the main reason behind rise of VTST above 400 Hz (Fig. 6). The shape of $v_{if}(t)$ and $v_{ifn}(t)$ ($v_{if}(t)$ added with neural noise $v_N(t)$) against 2 µm sinusoidal stimulus with frequency 50 to 3200 Hz are shown in Fig. 6. The subplot 4,2 of Fig. 6 indicates the typical receptor potential for mechanical noise ($x_N(t)$) alone (50 µm rms, Form Factor (FF) = 1.28 Crest Factor (CF) = 4.73). The $v_{if}(t)$ simulated from this model indicates that there is a little -ve phase if the stimulus amplitude and frequency is not very high (Fig. 5 subplot (1,2), Fig. 6 and 7), which is well matched with [26], [33]. The bottom envelop of ARPFM threshold ($v_t(t)$) bears an impression of the $v_{if}(t)$, or in other words, $v_t(t)$ rides on the $v_{if}(t)$. Similar impression is also observed in $v_s(t)$ if compared to $v_a(t)$, as described in [34]. Due to the inherent nature of ARPFM as described in method section, the potential of individual Na^+ and K^+ VAICs ($v_{nk}(t)$) (subplot 3,2), action potential ($v_a(t)$) (subplot 4,2) and the neural spike potential ($v_s(t)$) (subplot 5,2) show high level of temporal and

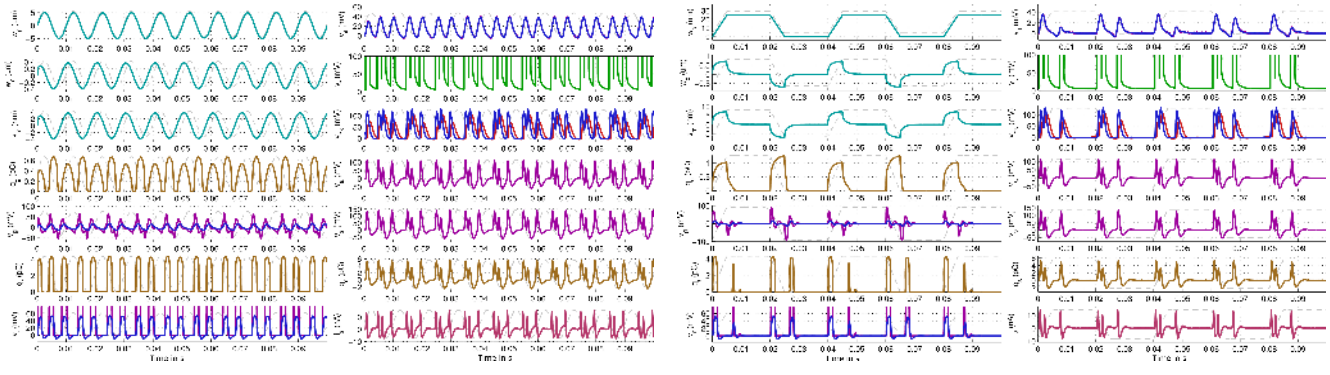

(A) (B)

Fig. 5. Morphological detail of neural response (100 ms frame) for **(A)** typical sinusoidal stimulus of (5 µm, 100 Hz), **(B)** typical trapezoidal stimulus of 25 µm, 25 Hz and period to rise-time ratio = 8; Left column: signals at receptive area of PC; Right column signals at 1st Ranvier's node of PC; X-axis: time in second; Y-axis (from top left column): x_s – Grey dotted waves in background representing the input stimulus at outer surface of skin (to indicate reference phase for signals), w_p – Compression at PC outermost layer, w_c – Compression at PC core layer, s_m – Stretch on PC neurite membrane, q_g – Net +ve charge transfer through SAICs, v_g – 1st stage generator potential along with its observable form (v_{gcf}). q_r – Net +ve charge transfer through VAICs, v_r – 2nd stage generator potential along with its observable form (v_{rf}). Compression at PC outermost layer; Y-axis (from top right column): v_{if} – Receptor potential at 1st Ranvier's Node along with its noisy form (v_{ifn}) due to added neural noise (v_N), v_t – Adaptive threshold of ARPFM, v_{nk} – Individual ionic potential of Na^+ and K^+ VAICs, v_a – Action potential, v_s – Neural spike at 1st Ranvier's node, q_a – Net +ve charge transfer through VAICs at 1st Ranvier's node, i_a – Current at 1st Ranvier's node.

morphological accuracy, as in [26], [34]. The plot of $q_s(t)$ and $i_s(t)$ represents the trans-membrane charge transfer and current at the 1st Ranvier's node. It is clearly observable that the height of $i_s(t)$ varies less compared to $v_s(t)$, therefore in the propagated action potential the impression of the receptor potential fades rapidly.

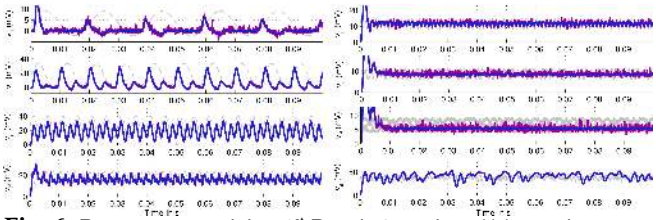

Fig. 6. Receptor potential at 1st Ranvier's node $v_{if}(t)$ (smoother trace in blue) and $v_{ifn}(t)$ (neural noise $v_N(t)$ added to $v_{if}(t)$, noisy trace in magenta) for different sinusoidal stimuli ($x_s(t)$) of amplitude 2 µm and frequency 50, 100, 200, 400, 800, 1600 and 3200 Hz in subplot 1,1 to subplot 3,2; In subplot 4,2 $v_{if}(t)$ and $v_{ifn}(t)$ for mechanical noise ($x_N(t)$) alone having amplitude 50 µm rms, Form Factor (FF) 1.28 and Crest Factor (CF) 4.73; Grey dotted waves in background representing the input stimulus at outer surface of skin (to indicate reference phase for signals); X-axis: time in second; Y-axis: voltage in mV.

Fig. 7 shows that near neurophysiological threshold (5 to 15 mV) of PC, AC component of the receptor potential rapidly increases along with DC and after the threshold the DC increases until $v_{ij}(t)$ saturates near 50 mV, which well matches with [33]. On the contrary, the AC of receptor potential significantly reduces above the threshold for >400 Hz stimulus.

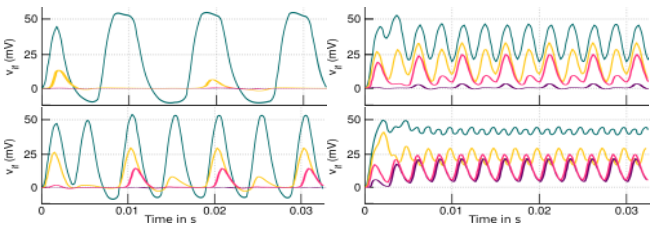

Fig. 7. AC & DC components of receptor potential for 0.5, 1, 2 & 64 µm sinusoidal stimuli; **Left** 50 & 100 Hz; **Right** 200 & 400 Hz.

Grouping of spikes: In comparison to sinusoidal signal (Fig. 5A), trapezoidal signal generates spikes against change in slope (at the corner points) of the stimulus (Fig. 5B). It is observed that the 2nd and 4th corner of the trapezoidal stimulus generates spike, only if the stimulus amplitude and slope is high enough, as they are originated by the overshoots of the $v_{gcj}(t)$. These spikes appears only if $Z_{SAIC}(s)$ contains under-damped poles (2) and membrane is modeled with 2nd order transfer function (4). Grouping of spikes in $v_s(t)$ is also observed for the sinusoidal stimulus (especially for low frequency (< 200 Hz) stimulus) if the stimulus amplitude remains several times higher than the VTST, as shown in Fig. 5A. When the spikes are grouped very closely, this model shows around 40% drop of the height of action potential [26], [34], which is actually caused by the sluggishness of the K^+ channel than the Na^+ channel as given in (9 and 10).

Variation of morphological parameters: As the generation of neural spike at 1st Ranvier's node mainly depends on the DC and AC components of the receptor potential ($v_{ij}(t)$), Fig. 8A shows how they get altered with the amplitude of $x_s(t)$. Apart from $v_{ij}(t)$, the AC_rms of core compression ($w_c(t)$) is also depicted in Fig. 8A. Variation of two more important morphological parameters (Form factor (FF) and Crest Factor (CF)) are shown in Fig. 8B. Near and below the threshold the AC component of $v_{ij}(t)$ dominates the DC component and near the threshold it shows a peak value, as shown in Fig. 8A. With further increase in amplitude of $x_s(t)$, the DC gradually increases whereas AC shows higher non-monotonic fluctuation around a saturation level. This behavior is observed over all the frequencies in this simulation and also in [26], [33]. As shown in Fig. 8B, the FF of $v_{ifn}(t)$ ($v_{ij}(t)$ added with neural noise) shoots up near threshold providing increased sensitivity in mechanotransduction. However CF remains higher even in sub-threshold range due to presence of the threshold in 1st stage 1st level nonlinear characteristics (Fig. 3A) and steep slope near the origin in the 1st stage 2nd level nonlinear characteristics (Fig. 3B).

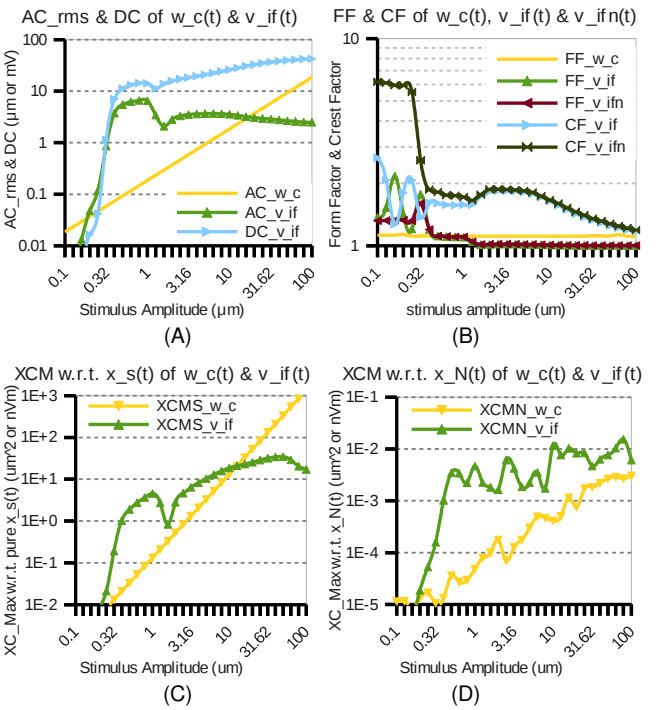

Fig. 8. Morphological properties of core compression (w_c), receptor potential (v_if) and v_ifn (v_if added with neural noise) w.r.t. stimulus amplitude ($x_s(t)$) for a typical frequency (400 Hz); **(A)** AC_rms and DC; **(B)** Form Factor (FF) and Crest Factor (CF); **(C)** Max. cross-correlation of w_c and v_if with pure input stimulus; **(D)** Max. cross-correlation of w_c and v_if with added mechanical noise $x_N(t)$. X-axis: stimulus amplitude equally spaced in dB scale.

Linear and nonlinear distortion: The core compression ($w_p(t)$) or the stretch signal at neurite membrane ($s_m(t)$) gets distorted in different stages of mechanotransduction while generating the receptor potential at 1st Ranvier's node ($v_{ij}(t)$) due to presence of linear frequency domain

filters ($Z_{SAIC}(s)$, $Z_{VAIC}(s)$, $T_{RI}(s)$ and $T_{R2}(s)$) and 3 nonlinear characteristics shown in Fig. 3. Therefore not only the stimulus but also the characteristics of mechanical noise ($x_N(t)$) significantly alters the mechanotransduction which is quantified by the maximum cross-correlation (XCM) of intermediate signals with the input stimulus $x_s(t)$ and mechanical noise $x_N(t)$ (Fig. 8 C and D). Similar to Fig. 8 A and B, XCM of Fig. 8 C also indicates resonating pattern near the threshold.

3.2 Noise in Mechanotransduction

In order to analyze effect of noise in mechanotransduction, we have first simulated the deterministic signals of all stages (both noise weight = 0 in Fig. 1) and referred as pure signal. Propagated noise is defined as the pure signal subtracted from actual signal. The variation of SNR for 400 Hz stimulus based on propagated noise is shown in Fig. 9A. From Fig. 9B it is clear that the propagated noise accumulates DC in mechanotransduction though both the additional noise ($x_N(t)$ and $v_N(t)$) are ideally zero-mean noise. This is mainly due to the nonlinear amplification in 2nd stage of the mechanotransduction. Therefore a very small amount of additional noise (even SNR > 150 at input stimuli) can shift the VTST significantly.

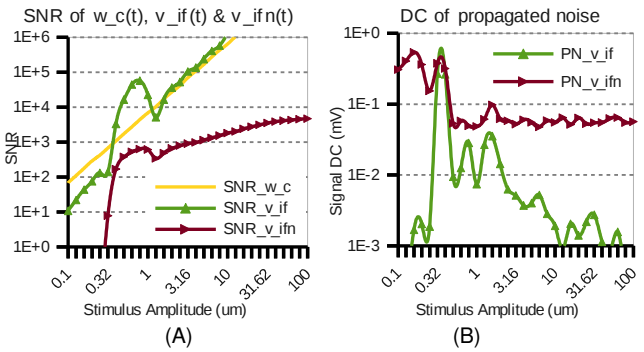

Fig. 9. **(A)** SNR based on pure signal (400 Hz) and propagated noise; **(B)** DC of propagated noise (PN) for v_if and v_ifn (v_if added with neural noise $v_N(t)$); X-axis: stimulus amplitude equally spaced in dB scale.

For studying PC neural response for random mechanical input, the amplitude (RMS) of additional mechanical noise ($x_N(t)$) of the input stage is increased till 100 µm by varying the noise weight (NW), as shown Fig. 1. During this simulation the amplitude of the mechanical stimulus ($x_s(t)$) is kept zero. This simulation has shown major difference in neural response of PC compared to sinusoidal stimulus (Fig. 8B) in form of morphology of receptor potential $v_{if}(t)$ and $v_{ifn}(t)$ (Fig. 10A). The characteristics in Fig. 10A shifted upward because the input signal being a random noise contains higher FF and CF. However it is interesting to observe that for random stimulus below the threshold, the FF and CF of both $v_{if}(t)$ and $v_{ifn}(t)$ drops (Fig. 10A), which oscillated or remained steady in case of a sinusoidal stimulus (Fig. 8B). This clearly represents the effect of stochastic resonance [40] due to nonlinear mechanotransduction which in turn reflects in the spike rate (SR) and MSDR characteristics of PC (narrow peak of MSDR near threshold Fig. 10A). The shape and gradual saturation of the SR vs. SA characteristics is also well matched with experimental data reported in [36]. The measurements reported in [36] are not calibrated below 0.5 µm and hence matching the exact value of threshold is beyond the scope of this paper. Therefore, slopes are given more importance in comparing the simulated spike rate results with the experimental ones.

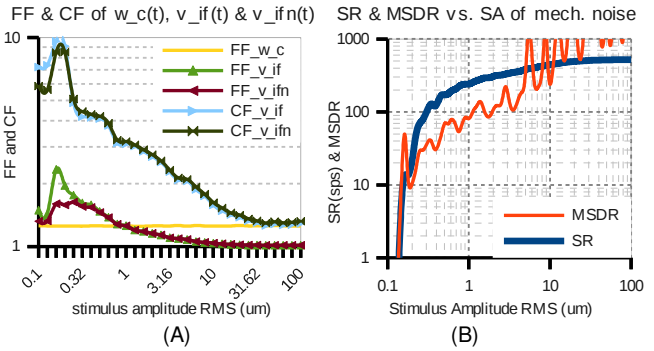

Fig. 10. Neural response of PC due to random excitation (mechanical noise $x_N(t)$) alone; **(A)** morphological properties of core compression (w_c) and receptor potential (v_if and v_ifn (v_if added with neural noise)) at 1st Ranvier's node in terms of Form Factor (FF) and Crest Factor (CF); **(B)** Average Spike Rate (SR) and MSDR of binary spike train ($v_{spk}(t)$); X-axis: Stimulus Amplitude RMS (SA) equally spaced in dB scale.

3.3 Spike rate vs. amplitude for sinusoidal input

In order to quantitatively validate our model response w.r.t. neurophysiological experimental results we have compared the variation of spike rate of $v_{spk}(t)$ (binary form of $v_s(t)$) with the [8], [36].

Plateau of spike rate characteristics: This model captures different plateaus of SR vs. SA characteristics (Fig. 11) which well matches with [36] as described below. For 25, 50, 100, 200, 400 Hz the 1:1 (1 spike for 1 stimulus cycle) plateau is clearly captured. For 400 Hz 2:1 plateau is absent. After a decade-long 1:1 plateau, the SR gradually saturates at 550 sps. For 50 Hz the 4:1 plateau appears immediately after 1:1 plateau, which is significantly wider. Similar skipping of plateau, 3:1 for 100 Hz and 2:1 for 200 Hz are also observed. A short width plateau of 1:2 is also observed for 400 Hz if MSDR is plotted w.r.t. amplitude of $x_s(t)$. However for 12.5 Hz the first short but significant width of plateau is observed at 3:1 followed by 4:1.

Saturation & nonmonotonicity of SR vs. SA characteristics: The saturation SR for >400 Hz stimulus is found to be higher than that of ≤400 Hz [8], [36]. All ≤400 Hz characteristics saturate below 500 sps and can be as low as 175 sps for 12.5 Hz stimulus (Fig. 11). The major nonmonotonicity observed in the simulation as well as in [8], [36], [41] is that after saturation SR falls with the increase of SA. Apart from this, for 800 Hz there is a small nonmonotonous range just after the steep rise of the characteristics

(Fig. 11B) which matches well with [36] for few of PCs. The depth of such nonmonotonicity becomes shallower with the increase of noise weight.

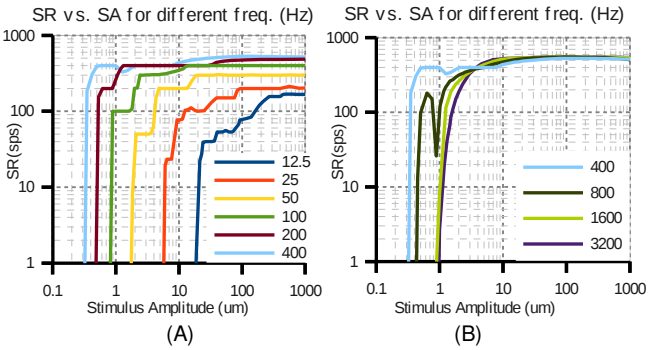

Fig. 11. Spike rate (SR) vs. stimulus amplitude (SA) characteristics considering (noise weight = 1 (Fig. 1)) starting from 12.5 to 3200 Hz and doubling in each step.

Slope of SR vs. SA characteristics in atonal interval: Fig. 12 shows that sensitivity index (α) of SR vs. SA characteristics (11) increases with the frequency till 400 Hz and slightly decreases after (Table 1). The terminal data points of each characteristic below 400 Hz (Fig. 12 A) are indication of absolute threshold (τ) and entrainment threshold (τ_e) for the corresponding frequencies. For above 600 Hz stimulus the SR vs. SA characteristics gradually saturates before reaching 1:1 plateau (Fig. 11 B), therefore in that frequency range the $\tau_e \to \infty$. Such saturation of SR around 600 sps is found to be true for most of the PCs. However in few rare cases SR can even reach 1000 sps [36].

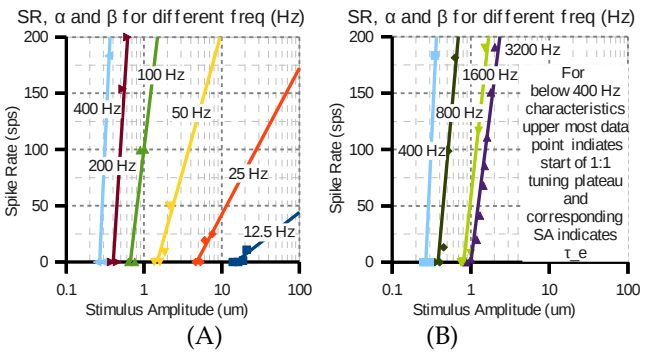

Fig. 12. Near threshold ($SR = \alpha\ log(SA/\tau);\ \beta = log(\tau)$) approximation (11); absolute and entrainment threshold (amplitude of lower and upper terminal data point threshold (τ & τ_e)) and sensitivity index (slope=α).

Accuracy of model response: The first level of model accuracy can be verified in terms of tuning plateaus of SR vs. SA characteristics compared to [36] (Fig. 11). In order to quantify the accuracy we have selected three parameters of the characteristics (Table 1): 1) absolute threshold (T), 2) entrainment threshold (T_e) and 3) near threshold sensitivity index (α), which shows a better match with [8], [36] over a wider spectrum than [17].

TABLE 1. ESTIMATED THRESHOLDS AND SENSITIVITY OF PC

Frq. (Hz)	Model			Model-[17]			Exp-[8]			Exp-[36]		
	α	T μm	T_e μm	α	T μm	T_e μm	α	T μm	T_e μm	α	T μm	T_e μm
25	56.6	4.8	7.4	61.4	60.0	90.0	35.9	10	20.0	48.7	1.5	2.0
100	247	0.7	1.0	131	2.8	6.0	212	0.5	0.8	246	0.2	0.3
400	637	0.3	0.6	-	0.3	inf	493	0.2	1.0	425	0.05	0.2
1600	272	0.8	inf	-	-	-	-	-	-	-	-	-

Variation of threshold due to noise level: In Fig. 13 shows how The absolute threshold of PC neural response depends on the mechanical noise (mechanical noise weight (NW) (Fig. 1) varied from 0 to 10) w.r.t. the shift of equal SR contour and equal MSDR contour. The down shift of SR=1 and MSDR=1 contour indicates that VTST at high frequency is highly noise dependent. Even a little noisy signal with SNR > 150 (NW=1) shifts the VTST above 400 Hz by 3 dB w.r.t. the deterministic VTST (NW=0).

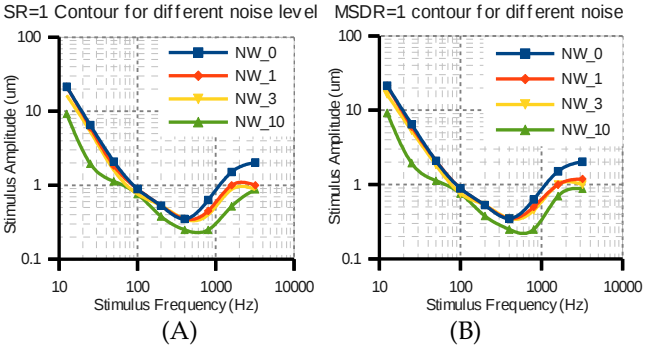

Fig. 13. (A) Variation of equal SR contour (SR=1) and **(B)** equal MSDR contour (MSDR=1) based on different levels of mechanical noise added to input stimulus $x_s(t)$ (Fig. 1); Noise weight (NW) = [0, 1, 3, 10].

4 DISCUSSION

The main motivation of this work is to investigate the increase of variabilities of psychophysical VTSTC above 400 Hz considering the position, slope, curvature, minimum (Fig. 14). Although the variabilities are partly due to site of stimulation or procedure of experiment, the focus of this paper is the variability in the slope of the characteristics above 400 Hz. Another motivation for us is to look into the ionic basis of the mechanotransduction in PC neurite. We have shown that there could be no distinctive upper bound of psychophysical VTST (Fig. 14) above 800 Hz as α becomes smaller and $\tau_e \to \infty$ in this frequency range for most PCs.

The developed nonlinear mechanotransduction model clearly describes that high frequency VTST is much more sensitive even to a small noise added to stimulus (Fig. 13) in comparison to low frequency VTST. Due to stochastic resonance it improves signal detectability by adding extra DC level to receptor potential although the mechanical noise itself does not contain any DC level. It is interesting to observe that the nonlinear mechanotransduction

makes the transduced mechanical noise (propagated $x_N(t)$ which was Gaussian in nature) resembling to the pulsating neural noise ($v_{NP}(t)$) (increase of CF in Fig. 10A).

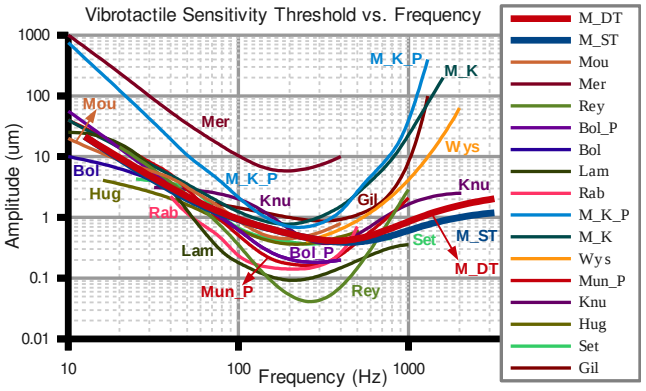

Fig. 14. Comparison of the VTSTCs estimated from model with experimental literature; M_DT and M_ST: Deterministic and stochastic estimation from the model, Mou: [7], Mer: [6], Rey: [10], Bol, Bol_P: [3], Lam: [5], Rab: [9], M_K, M_K_P: [42], Wys: [11], Mun_P: [8], Knu: [43], Hug: [44], Set: [45], Gil: [46]. The suffix "P" in the legend indicates the VTSTC of PC alone.

Apart from explaining the variation of VTSTC, the developed nonlinear mechanotransduction model is more generalized to capture the morphological details of receptor potential of PC neurite. This is achieved because each element of the model has either physiological or electrochemical interpretation rather than abstract approximation of input output relation. With the help of this model we propose that the VAICs present in axolemma and lamella membrane [19] acts as the nonlinear amplifier for the 1st stage of receptor potential generated by SAICs. This results in overshoot in Fig. 8 and 9 for the near threshold SA which is finally reflected in higher sensitivity index (α) (11) near the threshold.

The reason why SAICs needs higher order transfer function to approximate the membrane impedance is probably the variation of dielectric value due to changes in membrane thickness by the stimulus itself. Therefore if receptive area of PC neurite is excited by equivalent voltage signal, the morphology of the receptor potential at 1st Ranvier's node may show little difference. However the propagation of action potential due to electrical excitation after 1st Ranvier's node and mechanical excitation does not show much difference [34].

The spike generation at 1st Ranvier's node of PC is modeled with ARPFM which is accurate enough to capture the variation of spike height in refractory period, abortive T-spike [34], and grouping of neural spikes due the trapezoidal and low frequency sinusoidal stimulus (Fig. 5). The accuracy of the model can also be realized in terms of more realistic simulation of SR vs. SA characteristics than [15], which clearly captures the step-like, nonlinear, saturating and nonmonotonic patterns as found in experiments [36]. This model also captures the saturation of PC at higher amplitude for random excitation than for pure tone excitation, while the threshold still remains in the order of 0.1 - 0.2 µm rms [36] (Fig. 10).

The major limitation of this model is that the nonlinear characteristics and transfer functions are empirically estimated based on the ion channel characteristics in [24], [25], [29] and typical neural membrane impedance in [30], [31]. These characteristics are then approximated in order to match the experimental neural response in [8], [36]. Better approximation of these characteristics demands more number of parameters in ion channel model and therefore the desired accuracy of model is restricted in terms of the width of the 1st plateau of SR vs. SA characteristics. Apart from the approximation of ion channel characteristics the forms of intermediate signals proposed in this model need more experimental proof to confirm that the proposed transduction mechanism in reality describes the molecular basis of generation of receptor potential in PC which is not yet clearly understood [19].

In this paper we have not considered the variabilities of the of PC biomechanics like lamellae number, radius, depth in skin. If these variabilities are unified with this mechanotransduction model, it can simulate behaviour of a group of PCs revealing further insight towards perception of vibration through the somatosensory channel covering the speech spectrum. The simulated receptor potential not only matches with PC but also matches with that of hair cells [33] (Fig. 7). However restricting only to PC neural response and considering biomechanics of only 30 layers PC similar to [20], we have successfully explained many critical features of nonlinear stochastic mechanotransduction over a wide frequency band covering a significant range of speech spectrum.

REFERENCES

[1] O. Bau et al., "TeslaTouch: Electrovibration for Touch Surfaces," in *Proceedings of the 23Nd Annual ACM Symposium on User Interface Software and Technology*, New York, NY, USA, 2010, pp. 283–292.

[2] M. Rothenberg et al., "Vibrotactile frequency for encoding a speech parameter," *J. Acoust. Soc. Am.*, vol. 62, no. 4, pp. 1003–1012, 1977.

[3] S. J. Bolanowski, Jr. et al., "Four channels mediate the mechanical aspects of touch," *J. Acoust. Soc. Am.*, vol. 84, no. 5, pp. 1680–1694, Nov. 1988.

[4] F. A. Geldard, "The Perception of Mechanical Vibration: III. The Frequency Function," *The Journal of General Psychology*, vol. 22, no. 2, pp. 281–289, 1940.

[5] P. J. J. Lamore et al., "Envelope detection of amplitude-modulated high-frequency sinusoidal signals by skin mechanoreceptors," *J. Acoust. Soc. Am.*, vol. 79, no. 4, pp. 1082–1085, 1986.

[6] M. M. Merzenich and T. Harrington, "The sense of flutter-vibration evoked by stimulation of the hairy skin of primates: Comparison of human sensory capacity with the responses of mechanoreceptive afferents innervating the hairy skin of monkeys," *Exp. Brain Res.*, vol. 9, no. 3, pp. 236–260, 1969.

[7] V. B. Mountcastle et al., "Detection thresholds for stimuli in humans and monkeys: comparison with threshold events in mechanoreceptive afferent nerve fibers innervating the monkey hand," *J. Neurophysiol.*, vol. 35, no. 1, pp. 122–136, Jan. 1972.

[8] M. A. Muniak et al., "The Neural Coding of Stimulus Intensity: Linking the Population Response of Mechanoreceptive Afferents with Psychophysical Behavior," *J. Neurosci.*, vol. 27, no. 43, pp. 11687–11699, Oct. 2007.

[9] W. M. Rabinowitz et al., "Multidimensional tactile displays: Identification of vibratory intensity, frequency, and contactor area," *J. Acoust. Soc. Am.*, vol. 82, no. 4, pp. 1243–1252, 1987.
[10] D. D. Reynolds et al., "Hand-arm vibration, Part III: Subjective response characteristics of individuals to hand-induced vibration," *J. Sound Vibrat.*, vol. 51, no. 2, pp. 267–282, 1977.
[11] L. Wyse et al., "Perception of vibrotactile stimuli above 1kHz by the hearing-impaired," in *NIME '12*, University of Michigan, Ann Arbor, Michigan, USA, 2012.
[12] A. W. Freeman and K. O. Johnson, "Cutaneous mechanoreceptors in macaque monkey: temporal discharge patterns evoked by vibration, and a receptor model," *J. Physiol.*, vol. 323, no. 1, pp. 21–41, Jan. 1982.
[13] F. Grandori and A. Pedotti, "Theoretical Analysis of Mechano-to-Neural Transduction in Pacinian Corpuscle," *IEEE T. Biomed. Eng.*, vol. BME-27, no. 10, pp. 559–565, Oct. 1980.
[14] F. Grandori and A. Pedotti, "A mathematical model of the Pacinian corpuscle," *Biol. Cybern.*, vol. 46, no. 1, pp. 7–16, 1982.
[15] D. F. Liu, "Simulation Model of Pacinian Corpuscle for Haptic System Design," M.S. Thesis, Rochester Institute of Technology, Kate Gleason College of Engineering, Rochester, New York, 2011.
[16] S. Bensmaia et al., "Conveying tactile feedback using a model of mechanotransduction," presented at the BioCAS, IEEE, 2008, pp. 137–140.
[17] Y. Dong et al., "A simple model of mechanotransduction in primate glabrous skin," *J. Neurophysiol.*, vol. 109, no. 5, pp. 1350–1359, 2013.
[18] R. B. Northrop, *Introduction to dynamic modeling of neuro-sensory systems*. Boca Raton, Florida, USA: CRC Press, 2001.
[19] L. Pawson and S. J. Bolanowski, "Voltage-gated sodium channels are present on both the neural and capsular structures of Pacinian corpuscles," *Somatosens. Mot. Res.*, vol. 19, no. 3, pp. 231–237, 2002.
[20] A. Biswas et al., "A Biomechanical Model of Pacinian Corpuscle & Skin," in *Biomedical Science and Engineering Conference (BSEC)*, ORNL, Oak Ridge, TN, USA, 2013, pp. 1–4.
[21] A. Biswas et al., "Multiscale layered biomechanical model of pacinian corpuscle," *IEEE Trans. Haptics*, vol. Submitted for publication, 2014.
[22] J. Sherrick and E. Carl, "Variables affecting sensitivity of the human skin to mechanical vibration," *Journal of Experimental Psychology*, vol. 45, no. 5, pp. 273–282, May 1953.
[23] L. J. Drew et al., "Touch," in *Mechanosensitive Ion Channels, Part B*, vol. 59, O. P. Hamill, Ed. Academic Press, 2007, pp. 425 – 465.
[24] H. Cho et al., "Mechanosensitive Ion Channels in Cultured Sensory Neurons of Neonatal Rats," *J. Neurosci.*, vol. 22, no. 4, pp. 1238–1247, Feb. 2002.
[25] O. P. Hamill and B. Martinac, "Molecular Basis of Mechanotransduction in Living Cells," *physiol. Rev.*, vol. 81, no. 2, pp. 685–740, Apr. 2001.
[26] J. Bell et al., "The structure and function of pacinian corpuscles: A review," *Prog. Neurobiol.*, vol. 42, no. 1, pp. 79–128, Jan. 1994.
[27] A. Gomis et al., "Hypoosmotic- and pressure-induced membrane stretch activate TRPC5 channels," *J. Physiol.*, vol. 586, no. 23, pp. 5633–5649, Dec. 2008.
[28] W. Niu and F. Sachs, "Dynamic properties of stretch-activated K+ channels in adult rat atrial myocytes," *Prog. Biophys. Mol. Bio.*, vol. 82, no. 1–3, pp. 121 – 135, 2003.
[29] D. Schmidt et al., "Mechanistic basis for low threshold mechanosensitivity in voltage-dependent K+ channels," *PNAS*, vol. 109, no. 26, pp. 10352–10357, 2012.
[30] M. S. Awayda et al., "Frequency-Dependent Capacitance of the Apical Membrane of Frog Skin: Dielectric Relaxation Processes," *Biophys. J.*, vol. 76, no. 1, pp. 219–232, Jan. 1999.
[31] K. S. Cole and R. F. Baker, "Longitudinal impedance of the squid giant axon," *J. Gen. Physiol.*, vol. 24, no. 6, pp. 771–788, 1941.
[32] C. M. Checkosky and S. J. Bolanowski, "Effects of stimulus duration on the response properties of Pacinian corpuscles: Implications for the neural code," *J. Acoust. Soc. Am.*, vol. 91, no. 6, pp. 3372–3380, 1992.
[33] A. C. Crawford and R. Fettiplace, "Non-linearities in the responses of turtle hair cells," *J. Gen. Physiol.*, vol. 315, no. 1, pp. 317–338, 1981.
[34] W. R. Loewenstein and R. Altamirano-Orrego, "The refractory state of the generator and propagated potentials in a pacinian corpuscle.," *J. Gen. Physiol.*, vol. 41, no. 4, pp. 805–824, Mar. 1958.
[35] L. V. Chernomordik et al., "The electrical breakdown of cell and lipid membranes: the similarity of phenomenologies," *BBA-Biomembranes*, vol. 902, no. 3, pp. 360–373, Sep. 1987.
[36] S. J. Bolanowski and J. J. Zwislocki, "Intensity and frequency characteristics of pacinian corpuscles. I. Action potentials," *J. Neurophysiol.*, vol. 51, no. 4, pp. 793–811, Apr. 1984.
[37] G. Baranauskas and M. Martina, "Sodium Currents Activate without a Hodgkin and Huxley-Type Delay in Central Mammalian Neurons," *J. Neurosci.*, vol. 26, no. 2, pp. 671–684, Jan. 2006.
[38] C. L. V. Doren et al., "Vibrotactile temporal gap detection as a function of age," *J. Acoust. Soc. Am.*, vol. 87, no. 5, pp. 2201–2206, 1990.
[39] R. H. LaMotte and V. B. Mountcastle, "Capacities of humans and monkeys to discriminate vibratory stimuli of different frequency and amplitude: a correlation between neural events and psychological measurements," *Journal of Neurophysiology*, vol. 38, no. 3, pp. 539–559, May 1975.
[40] G. A. Gescheider et al., "Effects of noise on detection of amplitude increments of sinusoidal vibration of the skin," *J. Acoust. Soc. Am.*, vol. 91, no. 1, pp. 348–353, 1992.
[41] V. Sahai et al., "Processing of Vibrotactile Inputs From Hairy Skin by Neurons of the Dorsal Column Nuclei in the Cat," *J. Neurophysiol.*, vol. 95, no. 3, pp. 1451–1464, Mar. 2006.
[42] E. R. Kandel et al., *Principles of Neural Science*, 4th ed. New York, USA: McGraw-Hill, 2000.
[43] V. O. Knudsen, "'Hearing' with the Sense of Touch," *J. Gen. Psychol.*, vol. 1, no. 2, pp. 320–352, 1928.
[44] A. Hugony, "Über die Empfindung von Schwingungen mittels des Tastsinns," *Z. Biol.*, vol. 96, p. 584, 1935.
[45] W. Setzepfand, "Zur Frequenzabhängigkeit der Vibrationsemplindung des Menschen," *Z. Biol.*, vol. 96, pp. 236–240, 1935.
[46] B. von H. Gilmer, "The Measurement of the Sensitivity of the Skin to Mechanical Vibration," *The Journal of General Psychology*, vol. 13, no. 1, pp. 42–61, 1935.

Abhijit Biswas got his B.Tech. in Electronics and Instrumentation from University of Kalyani and M.E. in Biomedical Engineering from Jadavpur University, Kolkata in 2006 and 2008 respectively. He worked in Robhatah Robotic Solutions Pvt. Ltd., a spin-off company of National University of Singapore, as Sr. R&D Engineer for two years and joined TouchLab, IIT Madras as a research scholar in 2010.

M. Manivannan holds PhD and ME degrees from the Indian Institute of Science, Bangalore. He received post-doctoral training in Haptics at the MIT, Cambridge. Before MIT, he received another post-doctoral training in CAD standards and Sensors Network at the National Institute of Standards and Technology, Maryland. He served as a chief software architect of Yantric Inc. before joining IIT Madras in Jun, 2005.

M. A. Srinivasan is the director of MIT's Touch Lab and senior research scientist at MIT's Research Laboratory of Electronics. His research interests include haptic computation, cognition, and communication in humans and machines, particularly to enhance human–machine interactions in virtual environment systems. Srinivasan has a PhD in applied mechanics from the Department of Mechanical Engineering at Yale University.